Preprints.org

Article

Not peer-reviewed version

An Effective Near-Field to Far-Field Transformation with Planar Spiral Scanning for Flat Antennas under Test

Florindo Bevilacqua *, Francesco D'Agostino, Flaminio Ferrara, Claudio Gennarelli *, Rocco Guerriero, Massimo Migliozzi, Giovanni Riccio

Posted Date: 3 August 2023

doi: 10.20944/preprints202308.0288.v1

Keywords: antennas measurements; non-redundant sampling representations; planar spiral scanning; near-to-far-field transformations

Preprints.org is a free multidiscipline platform providing preprint service that is dedicated to making early versions of research outputs permanently available and citable. Preprints posted at Preprints.org appear in Web of Science, Crossref, Google Scholar, Scilit, Europe PMC.

Copyright: This is an open access article distributed under the Creative Commons Attribution License which permits unrestricted use, distribution, and reproduction in any medium, provided the original work is properly cited.

Preprints (www.preprints.org) | NOT PEER-REVIEWED | Posted: 3 August 2023 doi:10.20944/preprints202308.0288.v1

Disclaimer/Publisher's Note: The statements, opinions, and data contained in all publications are solely those of the individual author(s) and contributor(s) and not of MDPI and/or the editor(s). MDPI and/or the editor(s) disclaim responsibility for any injury to people or property resulting from any ideas, methods, instructions, or products referred to in the content.

Article

An Effective Near-Field to Far-Field Transformation with Planar Spiral Scanning for Flat Antennas under Test

Florindo Bevilacqua [1], Francesco D'Agostino [1], Flaminio Ferrara [1], Claudio Gennarelli [1,*], Rocco Guerriero [1], Massimo Migliozzi [1] and Giovanni Riccio [2]

[1] Dept. of Industrial Engineering, University of Salerno, via Giovanni Paolo II, 84084 Fisciano, Italy; fbevilacqua@unisa.it; fdagostino@unisa.it; flferrara@unisa.it; cgennarelli@unisa.it; rguerriero@unisa.it; mmigliozzi@unisa.it

[2] Dept. of Information and Electrical Engineering and Applied Mathematics, University of Salerno, via Giovanni Paolo II, 84084 Fisciano, Italy; griccio@unisa.it

* Correspondence: cgennarelli@unisa.it; Tel.: +39-089-96-4280

Abstract: Goal of this article is to provide the numerical and experimental assessments of an effective near-field to far-field transformation (NF–FF T) technique with planar spiral scanning for flat antennas under test (AUTs), which requires a non-redundant, i.e., minimum, amount of NF measurements. This technique has its roots in the theory of non-redundant sampling representations of electromagnetic fields and has been devised by suitably applying the unified theory of spiral scans for non-volumetric antennas to the case in which the considered AUT is modeled by a circular disk having its radius equal to one half the AUT maximum dimension. It makes use of a 2-D optimal sampling interpolation (OSI) formula to accurately determine the massive NF data required by the classical plane-rectangular NF–FF T technique from the non-redundant ones gathered along the spiral. It must be emphasized that, when considering flat AUTs, the developed transformation allows to further and significantly save measurement time as compared to that needed by the previously developed NF–FF T techniques with planar spiral scans based on the quasi-planar antennas modelings, because the number of turns of the spiral and that of NF data to be acquired depend somehow on the area of the modeling surface. The reported numerical simulations assess the accuracy of the proposed NF–FF T technique, whereas the experimental tests prove its practical feasibility.

Keywords: antennas measurements; non-redundant sampling representations; planar spiral scanning; near-to-far-field transformations

1. Introduction

Antenna measurements concerning the pattern representation of a source under test need to reduce the time devoted to the data collection for increasing the number of tests in the available time slot. This target can be accomplished in the far-field (FF) region as well as in the near-field (NF) volume surrounding the antenna under test (AUT) by adopting strategies, which allow: a) the reduction of the data to acquire and b) the adoption of non-conventional scanning techniques not requiring a step-by-step acquisition. The requirement a) can be satisfied by resorting to the theoretical results concerning the non-redundant sampling representation of the electromagnetic (EM) field [1,2] radiated by antennas, whereas on-the-fly data acquisition permitted by the continuous movements of positioners can be used to fulfill the requirement b).

A non-redundant sampling representation of the EM field radiated by the AUT permits to determine the field value at any observation point on surfaces in the NF or FF region by employing the minimum number of data [1,2] available on the same surface. Such data can be properly expended in optimal

© 2023 by the author(s). Distributed under a Creative Commons CC BY license.

Preprints (www.preprints.org) | NOT PEER-REVIEWED | Posted: 3 August 2023 doi:10.20944/preprints202308.0288.v1

sampling interpolation (OSI) algorithms to recover the needed field values. Such a procedure is extremely convenient when dealing with NF data to be used in NF–FF transformation (NF–FF T) techniques [3–11]; f.i., in the non-redundant NF–FF T techniques with plane-rectangular [12,13], plane-polar [14–17], and bi-polar [18,19] scannings, efficient OSI algorithms have been proposed to precisely recover the NF data necessary for the standard plane-rectangular NF–FF T technique [20,21].

Innovative and non-conventional NF spiral scans based on a Rahmat-Samii's idea [22] consent on-the-fly data gathering by adopting the continuous and synchronized movements of the positioners driving AUT and measuring probe. In particular, NF–FF Ts using sampling points on a planar spiral have been developed to reduce the acquisition time [23–26]. This reduction is accomplished accounting for the theory of the non-redundant sampling representations [1,2] and for the unified theory of the spiral scannings for volumetric [27] and non-volumetric AUTs [28,29]. In fact, the number of spiral turns required to cover a given scanning area decreases since its step must satisfy the non-redundant sampling rule associated to a radial line, and the number of sampling points on the resulting spiral is the minimum one. It must be also emphasized that the percentage of reduction depends on the area of the closing surface Σ adopted to model the antenna [1], f.i., by assuming as standard AUT modeling the spherical surface with radius equal to the AUT half-dimension, the numbers of spiral turns and sampling points decrease if an oblate spheroid, which is enclosed in the above spherical surface, is used as AUT modeling [25,26]. On the other end, a two-bowls (i.e., a surface formed by two circular bowls with the same aperture and lateral bends which may differ) can represent the best choice in the case of quasi-planar AUTs [26], as it generally permits a better fitting of their shape.

The following question now arises. Is it possible to lower the number of spiral turns and the number of the corresponding samples points in the case of a flat AUT? The answer is described in next sections of this article, which is organized as follows. The theoretical analysis is given in Section 2 by employing a disk with radius equal to the AUT half-dimension as AUT model. Section 3 is devoted to numerical tests and comparisons with measured data. Conclusions are collected in Section 4.

2. OSI REPRESENTATION ON A PLANE FROM SPIRAL SAMPLES

The proposed acquisition strategy is introduced in this Section, as well as the formulation of the innovative disk modeling for flat antennas and the related OSI formulas.

It is supposed to perform the characterization of a flat AUT by the means of a planar spiral NF facility, which acquires the NF voltages over a plane set at distance d from it. Furthermore, it is assumed to adopt an electrically small, first order probe, namely a probe whose FF pattern has a first-order azimuthal dependence, to carry out the acquisition of the required data. Such an assumption will be properly exploited in the following. Moreover, it is also convenient to introduce a spherical and a Cartesian reference coordinate system, (r, ϑ, φ) and (x, y, z), both with their centers at O, to specify an observation point P. Such a point can be identified on the scanning plane by the plane-polar coordinates (ρ, φ), as depicted in Figure 1.

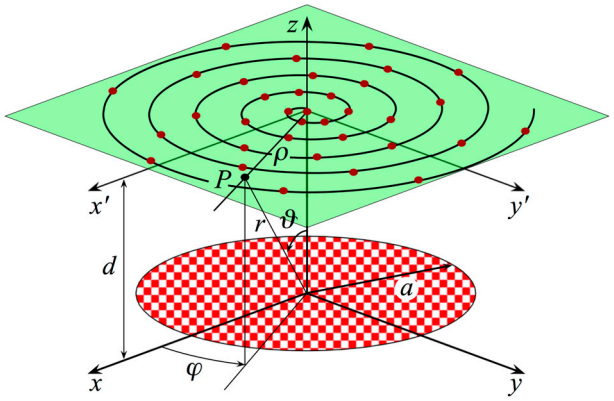

Figure 1. Relevant to the planar spiral scan for a flat antenna.

Preprints (www.preprints.org) | NOT PEER-REVIEWED | Posted: 3 August 2023 doi:10.20944/preprints202308.0288.v1

It is interesting to note as the voltage revealed at the output terminals of the considered scanning probe shows the same effective spatial bandwidth as the field [15]. Such a property allows one to apply the results presented in [1] also to the acquired voltage. Accordingly, a convenient representation of the voltage over any curve Γ of the plane, can be properly formulated by describing such a curve by an opportune parameter ξ and referring to the "reduced voltage"

$$\tilde{V}(\xi) = V(\xi)\, e^{j\gamma(\xi)} \tag{1}$$

wherein $\gamma(\xi)$ denotes an opportune phase function to be calculated and the voltage V is equal to $V_\varphi(\xi)$ or $V_\rho(\xi)$ depending on whether the probe is in the nominal orientation or rotated by π/2. According to [1], V is a function spatially quasi bandlimited to W_ξ. Anyhow, it can be very well approximated by a function bandlimited to $\chi' W_\xi$, by properly setting the excess bandwidth factor χ' which makes possible to control the aliasing error. It should be noted as a χ'-value a slight greater than one can be suitably used when dealing with the characterization of electrically large AUTs [1].

By following the reasoning derived in [28], it is possible to reconstruct the voltage distribution efficiently and accurately over the acquisition plane from a reduced set of NF data gathered on the spiral, by applying a 2-D OSI formula. The OSI scheme can be derived [28] by enforcing that the spiral step is the same of the sampling spacing necessary to perform the interpolation on a radial line. After that, a suitable non-redundant sampling representation over this spiral is formulated.

As shown in [1], the parameter to be employed to provide the optimal representation along radial lines, the associated phase function and spatial bandwidth are given by:

$$\xi = (\pi / \ell')\left[R_1 - R_2 + s'_1 + s'_2\right] \tag{2}$$

$$\gamma = (\pi / \lambda)\left[R_1 + R_2 + s'_1 - s'_2\right] \tag{3}$$

$$W_\xi = \ell' / \lambda \tag{4}$$

where ℓ' denotes the length of Γ' (intersection curve between the meridian plane at the observation point P and Σ), λ is the wavelength, R_1 and R_2 are the distances from P to the tangency points P_1 and P_2 on such a curve, and s'_1 and s'_2 are their curvilinear abscissae.

The relations (2)–(4) are general and, to find their explicit expressions, it is necessary to specify the modeling surface Σ containing the AUT. It is important to highlight as the number N_S of samples at Nyquist rate on an arbitrary closed surface (even unbounded), which encircles the antenna, can be expressed as

$$N_S \cong \frac{\text{area of } \Sigma}{(\lambda/2)^2} \tag{5}$$

Therefore, it is evident as, by properly choosing the antenna modeling, it is possible to minimize the overall amount of needed NF data. In fact, a convenient approach to cut the number of required NF samples is to minimize the area of the surface modeling the antenna, by choosing a geometry which must fit very well the source shape so reducing the volumetric redundancy.

As a result, when considering flat antennas, the modeling surface to which corresponds the smallest area is that of a disk with radius a equal to half their maximum size, as it is capable to shape as far as possible their geometry. It should be noticed that the NF data reduction achievable by using such a modeling is much greater than that resulting in such a case from the usage of the previously derived models for quasi-planar antennas (two-bowls or oblate spheroid), which involve a residual volumetric redundancy.

By shaping the AUT with a disk of radius a, since (see Figure 2) $\ell' = 4a$, $s'_1 = -a$, and $s'_2 = a$ relations from (2) to (4) can be particularized as:

Preprints (www.preprints.org) | NOT PEER-REVIEWED | Posted: 3 August 2023 doi:10.20944/preprints202308.0288.v1

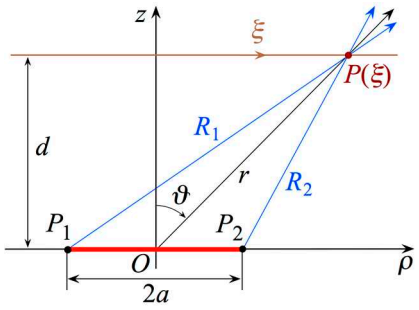

Figure 2. Geometry relevant to a radial line.

$$\xi = (\pi/4a)(R_1 - R_2) \tag{6}$$

$$\gamma = (\pi/\lambda)(R_1 + R_2 - 2a) \tag{7}$$

$$W_\xi = 4a/\lambda \tag{8}$$

As shown in [28], the spiral lying on the scanning plane can be achieved as projection through the curves at ξ= constant (Figure 3) of a spiral which wraps with a proper step the disk modeling the source.

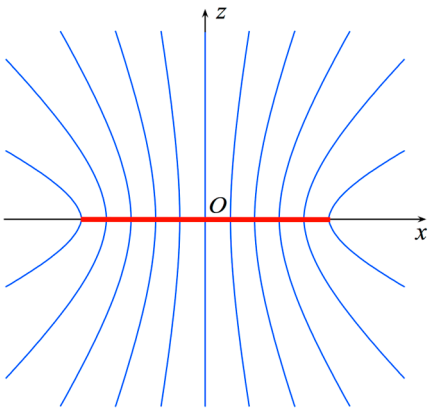

Figure 3. Curves at ξ= constant.

This step must coincide with the sampling spacing necessary to carry out the interpolation along a radial line, namely $\Delta\xi = 2\pi/(2N''+1)$, where $N'' = \mathrm{Int}(\chi N'+1)$, $N' = \mathrm{Int}\left(\chi' W_\xi + 1\right)$, $\mathrm{Int}(x)$ denotes the integer part of x, and $\chi > 1$ is the oversampling factor to be used for controlling the truncation error [1]. Therefore, the equations describing the acquisition spiral are:

$$\begin{cases} x = \rho(\xi)\cos\phi \\ y = \rho(\xi)\sin\phi \\ z = d \end{cases} \tag{9}$$

wherein ϕ denotes an angular parameter that allows to describe the spiral, $\rho(\xi) = d\tan\theta(\xi)$, and $\xi = k\phi$. Now, as two successive intersections at $Q(\phi)$ and $Q(\phi + 2\pi)$ of the considered radial line with the spiral determine its step, then, it results $k = 1/(2N''+1)$ [28]. At last, it is highlighted as the spiral angle θ, at variance with the zenithal angle ϑ, can be also negative, ranging. Furthermore, it is pointed out as the parameter ϕ is always continuous, whereas the azimuthal angle φ shows a discontinuity jump of π at the pole.

The unified theory of spiral scanning [28] is now exploited to develop the non-redundant representation on the spiral, namely, the optimal parameter η and the related phase function ψ. More in details, the parameter η for representing the spiral path must be equal to $2\pi/(\lambda W_\eta)$ times the curvilinear

Preprints (www.preprints.org) | NOT PEER-REVIEWED | Posted: 3 August 2023 doi:10.20944/preprints202308.0288.v1

abscissa of the projection point, which lies on the spiral which wraps the disk surface Σ. Furthermore, the associated phase function ψ needs to be the same of the one (γ) derived for a radial line. As concerns the spatial bandwidth W_η, it can be suitably calculated by imposing that the parameter η covers a 2π range when drawing the entire (closed) projecting spiral. Accordingly, W_η results to be $2/\lambda$ times the length of the spiral that wraps the disk from pole to pole [28].

In consideration of the aforementioned results, a fast and accurate way to reconstruct the voltage at the point *P*, on the radial line at φ, is to employ the following OSI formula [25,28]

$$V(\xi(\rho),\varphi) = \mathrm{e}^{-\mathrm{j}\gamma(\xi)} \sum_{n=n_0-q+1}^{n_0+q} \tilde{V}(\xi_n)\, OS\left(\xi, \xi_n, N, N'', \bar{\xi}\right) \tag{10}$$

where $2q$ *is* the number of retained intermediate reduced voltage samples $\tilde{V}(\xi_n)$, i.e. those in correspondence of the points of intersection of the acquisition spiral with the radial line passing through *P*, $\bar{\xi} = q\Delta\xi$, $N = N'' - N'$, and $n_0 = \mathrm{Int}[(\xi - \xi_0)/\Delta\xi]$,

$$\xi_n = k\varphi + n\Delta\xi = \xi_0 + n\Delta\xi \tag{11}$$

are the sampling points. In equation (10),

$$OS\left(\xi, \xi_n, N, N'', \bar{\xi}\right) = \mathrm{TS}_N\left(\xi - \xi_n, \bar{\xi}\right) D_{N''}(\xi - \xi_n) \tag{12}$$

is the OSI kernel function [1,28], wherein

$$TS_N(\xi, \bar{\xi}) = \frac{T_N\left[2\cos^2(\xi/2)/\cos^2(\bar{\xi}/2) - 1\right]}{T_N\left[2/\cos^2(\bar{\xi}/2) - 1\right]} \tag{13}$$

is the Tschebyscheff sampling function, $T_N(\xi)$ being the *N* degree Tschebyscheff polynomial, and

$$D_{N''}(\xi) = \frac{\sin\left[(2N''+1)\xi/2\right]}{(2N''+1)\sin(\xi/2)} \tag{14}$$

is the Dirichlet function.

By properly taking into account the non-redundant representation on the scanning spiral, is possible to determine [25,28] the intermediate reduced voltage samples $\tilde{V}(\xi_n)$ from the ones collected on the spiral through the OSI expansion:

$$\tilde{V}(\eta(\xi_n)) = \sum_{m=m_0-p+1}^{m_0+p} \tilde{V}(\eta_m)\, OS\left(\eta(\xi_n), \eta_m, M, M'', \bar{\eta}\right) \tag{15}$$

where $m_0 = \mathrm{Int}\left[\eta(\xi_n)/\Delta\eta\right]$, $2p$ represents the number of considered NF samples on the spiral, $\bar{\eta} = p\Delta\eta$, $M'' = \mathrm{Int}(\chi M' + 1)$, $M = M'' - M'$, $M' = \mathrm{Int}\left(\chi' W_\eta + 1\right)$,

$$\eta_m = m\Delta\eta; \qquad \Delta\eta = 2\pi/(2M''+1) \tag{16}$$

and the meaning of the other symbols is fairly similar to the ones in (10).

It is noteworthy that when applying the expansion (15) to recover the intermediate samples nearby the pole $\vartheta = 0$, even little changes of η entail large changes of the angular parameter ϕ. As a consequence, the bandwidth excess factor χ' to be used in (15) must be locally suitably increased to prevent that the increase of the band-limitation error in this zone can impair the accuracy and the quality of the reconstruction.

The 2-D OSI expansion, allowing the evaluation of the voltage distribution on the plane from the non-redundant samples gathered on the spiral, is finally obtained by matching the 1-D expansions (10) and (15). It is conveniently exploited to recover the voltage value of V_φ and V_ρ at the sampling positions of the regular Cartesian grid required for executing the NF–FF T [21]. Unfortunately, the relations in [21], accounting for the effects of the probe, enforce as entry the voltages V_x and V_y in

Preprints (www.preprints.org) | NOT PEER-REVIEWED | Posted: 3 August 2023 doi:10.20944/preprints202308.0288.v1

order to be applied. This entails that is necessary to perform the co-rotation of the probe during the measurement stage, such that its axes are maintained parallel to those of the AUT. However, this "hardware" co-rotation can be avoided by using, as already mentioned, a probe radiating a FF pattern showing only an azimuthal dependence of the first-order as, e.g., it occurs with a very close approximation for an open-ended rectangular waveguide excited by a TE_{10} mode [30]. As a matter of fact, in this case, the voltages V_x and V_y, which would be measured by the probe and the rotated one with co-rotation, can be calculated from the measured non-corotated ones, V_ρ and V_φ, by simply applying the relations

$$V_y = V_\varphi \cos\varphi - V_\rho \sin\varphi\,; \qquad V_x = V_\varphi \sin\varphi + V_\rho \cos\varphi \tag{17}$$

3. RESULTS

An extensive number of numerical simulations and experimental tests, performed at the Antenna Characterization Lab of the University of Salerno (UNISA), has been performed to thoroughly assess the precision and reliability of the developed non-redundant spiral NF–FF T for flat antennas.

3.1. Numerical tests results

We show, in this section, numerical results that proof the efficacy of the developed NF–FF T technique adopting a planar spiral scan. The considered AUT is a uniform circular planar array with radius $a = 21.0\,\lambda$. The array has been placed in the xy plane of the used reference system, as illustrated in Figure 1. The elements are elementary Huygens sources linearly polarized along the y-axis. They are symmetrically located with respect to the axes and are spaced azimuthally by approximately $0.7\,\lambda$ along circumferences, which are radially spaced by $0.7\,\lambda$. Furthermore, they have been fed in such a way that the AUT shows radiating characteristics somehow similar to a Tschebyscheff array, with a first side lobe level of –40 dB. According to the proposed sampling representation, the AUT is assumed to be enclosed within a disk of identical radius a. The NF samples of V_φ and V_ρ have been numerically evaluated as collected by an open-ended WR-90 rectangular waveguide on a spiral, which covers a circle with radius $\approx 71\,\lambda$ on a plane $d = 8.0\,\lambda$ away from the antenna center.

The accuracy of the 2-D OSI scheme, got by combining formulas (10) and (15), can be qualitatively and quantitatively assessed. From the qualitatively point of view, Figures 4 and 5 show the comparisons of the reconstructed amplitudes and phases with the exact ones relevant to V_φ and V_ρ along the radial lines at $\varphi = 0$ and $\varphi = \pi/2$, respectively. It is evident as the reconstructions, both for the amplitudes and phases, match very well the references. It must be underlined that these successful recoveries have been achieved by using an excess bandwidth factor $\chi' = 1.20$, which ensures a negligible band- limitation error [11], and $p = q = 7$ together with an oversampling factor $\chi = 1.20$ to control the truncation one. Moreover, to prevent the increase of the band-limitation error in the neighborhood of the pole, the χ' value employed in the interpolation on the spiral has been locally increased in such a way that in the zone of the spiral specified by the 32 samples near the pole, the sample spacing is reduced by a factor 11. Thus, the total number of NF samples on the spiral is 11 959, inclusive of the 320 "extra samples" at reduced spacing around the pole. It is also interesting to provide quantitative proofs of the precision of the 2-D OSI formula. To this end, the values of V_ρ, calculated through the 2-D OSI formula at the points of a close lattice in the central zone of the scan plane (to make sure the availability of the guard samples), have been compared with the exact values. This comparison has been carried out by choosing $\chi' = 1.20$ and different values of χ, p, and q. The resulting mean-square and maximum reconstruction errors, normalized to the maximum value of the voltage on the plane, are shown in Figure 6. It is evident that, by increasing the value of χ, p, and q, the reconstruction errors decrease. This provides a criterion to select the appropriate values of the OSI parameters, once the tolerable level of reconstruction error has been fixed.

Preprints (www.preprints.org) | NOT PEER-REVIEWED | Posted: 3 August 2023 doi:10.20944/preprints202308.0288.v1

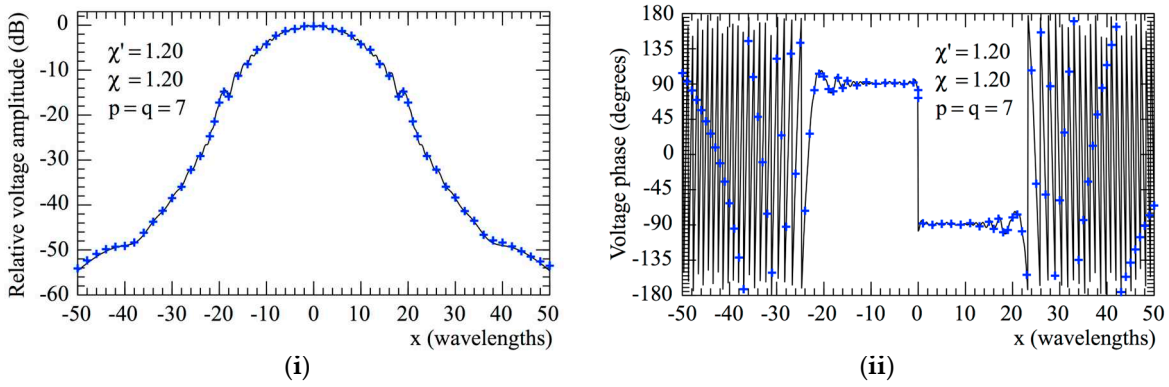

Figure 4. V_φ on the radial line at $\varphi = 0$. ——— reference. ++++ evaluated from the planar spiral NF measurements: (**i**) Amplitude; (**ii**) Phase.

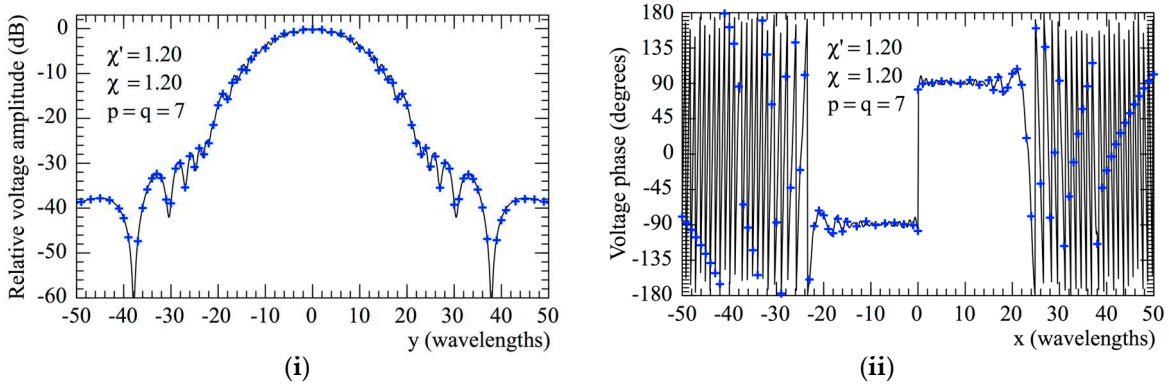

Figure 5. V_ρ on the radial line at $\varphi = \pi/2$. ——— reference. ++++ evaluated from the planar spiral NF measurements: (**i**) Amplitude; (**ii**) Phase.

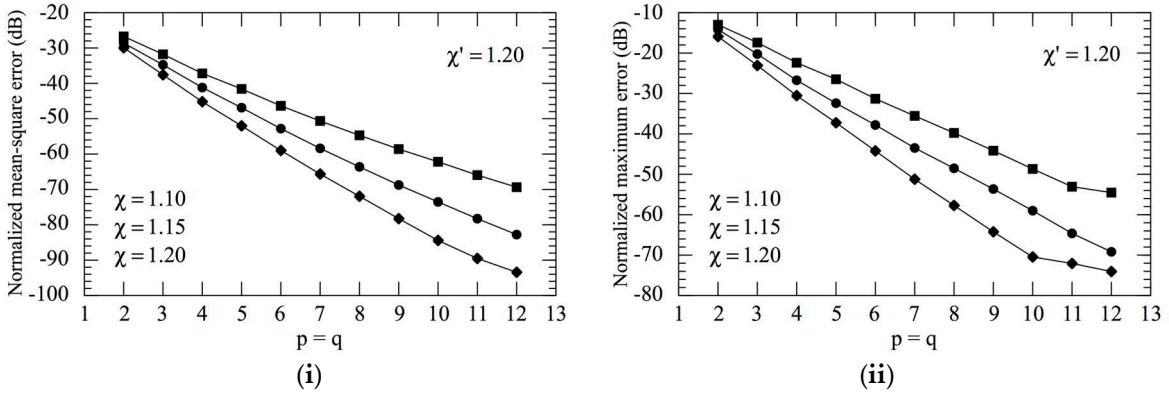

Figure 6. Errors in the evaluation of V_ρ. (i) Mean-square error, (ii) maximum error.

Finally, to evaluate the total efficacy of the proposed NF–FF T technique, the 2-D OSI formula has been used to precisely evaluate the voltages V_φ and V_ρ at the points of the Cartesian grid required to execute the standard Leach & Paris's NF–FF T technique [21]. Then, it is possible to exploit the Equations (17) to determine the corresponding needed values of V_x and V_y, since, as formerly stressed, the utilized probe radiates, with a very good approximation [30], a far field with a first-order azimuthal dependence. The E-plane and H-plane radiation patterns obtained from the 40 401 NF data reconstructed on the 0.5λ spaced square grid having a side length of 100λ, which is inscribed in the scanning circle, are compared to the exact ones in Figure 7. As can be noticed, the agreement of the so obtained FF patterns with the exact ones is very good also in the far out sidelobes region.

Preprints (www.preprints.org) | NOT PEER-REVIEWED | Posted: 3 August 2023 doi:10.20944/preprints202308.0288.v1

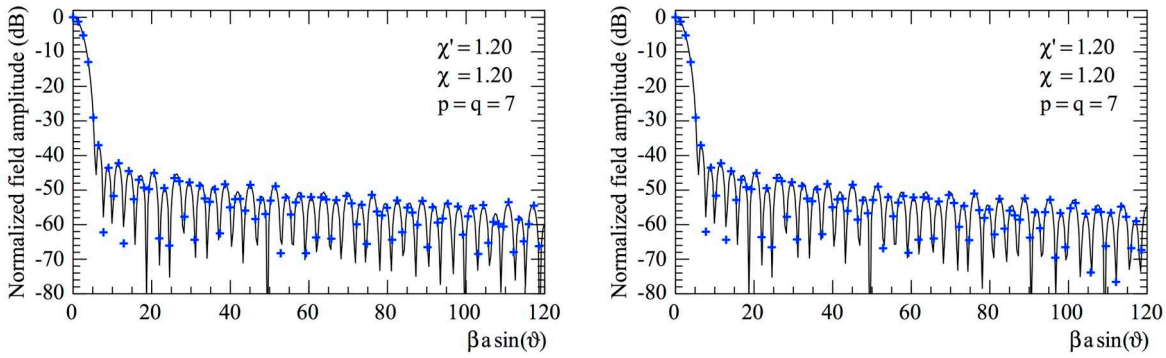

Figure 7. Far-field patterns. ——— exact. ++++ reconstructed from the non-redundant samples: (**i**) E-Plane; (**ii**) H-plane.

Before concluding the numerical section, it is interesting to highlight the data reduction obtained by employing the disk modeling of the AUT. To this end, Table 1 reports the comparison of the NF samples required to the various approaches to cover the scanning area of $100\lambda \times 100\lambda$. Interestingly, the proposed approach entails a significant reduction in the amount of NF samples as compared to the Leach & Paris's NF–FF T technique [21] as well as with respect to the classical plane-polar NF–FF T technique by Rahmat-Samii *et al*. [31,32]. Also, the number of data in the devised approach compares favorably with respect to the number of samples necessary to execute the NF–FF Ts with planar spiral scanning which adopt an oblate spheroid [25,26] or a two-bowls [26] modeling of the AUT. In particular, the oblate spheroid considered in the comparison has its semi-minor and semi-major axes equal to 21⌊ and 6⌊, respectively, whilst, the double-bowl has its aperture radius equal to 21⌊ and the radii of the lower and upper lateral bends both equal to 2.5⌊. At last, the use of the disk as AUT modeling results computationally much more simple than these latter, since all the expressions of the parameters involved in the representation are simpler. This highlights the efficiency and effectiveness of the proposed approach in reducing the amount of needed data, while keeping performance comparable to previous methods.

Table 1. NF data necessary for the various NF–FF T techniques.

Plane-rectangular NF–FF T [21]	Plane-polar NF–FF T [31,32]	Planar spiral NF–FF T [25,26] Oblate spheroid	Planar spiral NF–FF T [26] Double bowl	Planar spiral NF–FF T Disk
40 401	126 665	13 994	13 540	11 959

3.1. Experimental tests results

Some results of experimental tests which assess the validity of the here proposed NF–FF T technique with planar spiral scan are presented in the following. The experimental tests have been carried out at the laboratory of antenna characterization of the University of Salerno. This laboratory is supplied with an anechoic chamber 8 m × 5 m × 4 m sized, covered by pyramidal absorbers, which guarantee a reflectivity level lower than –40 dB. It is equipped with a "versatile" NF acquisition setup that offers the capability of performing spherical, cylindrical, plane-polar, and spiral scans, including the proposed scanning along a planar spiral. To perform the plane-polar scanning and, hence, the planar spiral one, the probe is attached to a vertical slide and the AUT is placed on a turntable with its axis perpendicular to the vertical slide. To expand the capabilities of the plane-polar NF facility, an additional rotary table is located between this positioner and the probe. Accordingly, this setup makes possible to acquire the NF data that would be typically measured using plane-rectangular NF setups. Furthermore, this additional rotating table permits the measurement of the NF data that would be gathered in a planar spiral NF setup with hardware co-rotation, where the axes of the probe and the AUT are kept parallel in the acquisition process. A pictorial illustration of the acquisition set-up is shown in Figure 8. A vector network analyzer is used to accomplish the measurement of amplitude and phase of the voltages collected by the

Preprints (www.preprints.org) | NOT PEER-REVIEWED | Posted: 3 August 2023 doi:10.20944/preprints202308.0288.v1

employed probe, an open-ended WR-90 rectangular waveguide. As previously observed, this choice allows the software co-rotation of the acquired voltage values, by using equations (17).

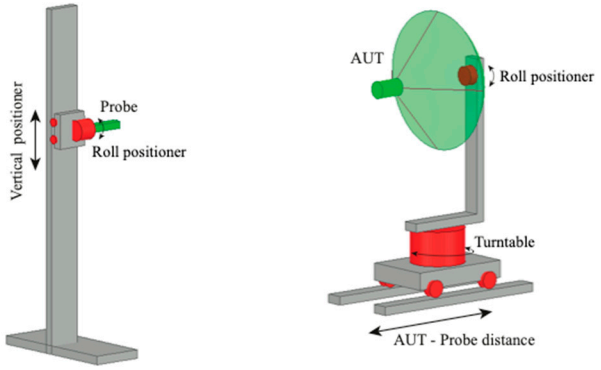

Figure 8. Pictorial illustration of the "versatile" NF setup existing at the UNISA Antenna Characterization Laboratory.

The AUT, a monopulse antenna in E-plane working at 10 GHz in the sum mode, is realized by assembling two pyramid-shaped horns, fed by a hybrid Tee. The aperture of each horn, placed on the plane xy, has sizes $8.9\,\mathrm{cm}\times 6.8\,\mathrm{cm}$ and the apertures centers are 26.5 cm away. According to the derived representation, this source is properly modeled by considering a disk with diameter $2a = 37.2$ cm. The distance d between the measurement plane and the probe is 16.5 cm and the samples of the probe voltages V_ρ and V_φ are acquired along a spiral which covers a circle with radius 114 cm. The sampling positions on the spiral have been determined in accordance with the derived non-redundant sampling representation by choosing $\chi = 1.25$ and a χ' value equal to 1.30 save for the interpolation along the spiral in the zone specified by the 24 samples nearby the pole, where it has been locally augmented such that the sample spacing is reduced exactly by a factor 9. Thus, the total number of the NF measurements on the spiral is 1665, inclusive of the 192 "extra samples" at reduced spacing nearby the pole.

To assess the accuracy of the 2-D OSI formula, the magnitudes and phases of the reconstructed voltages V_φ and V_ρ, along the radial lines at $\varphi = 0$ and $\varphi = \pi/2$, respectively, are compared in Figures 9 and 10 to those directly measured (references) along these radial lines. To provide a comprehensive analysis, Figure 11 presents the reconstructions of the amplitudes of V_φ and V_ρ on the radial line at $\varphi = \pi/6$. It can be clearly observed the very good matching of the measured voltages (solid line) with the interpolated ones (crosses). Some discrepancies result only for the more peripheral zones of the scan plane, characterized by very low voltages (lower than −50 dB). Furthermore, the interpolated voltages show a behavior which is smoother than that of the directly acquired voltages, which, on the other hand, appears rippled. This phenomenon occurs because the Dirichlet and Tscheby-scheff Sampling functions, kernel of the OSI expansions, allow one to reject the noise spatial harmonics greater than the antenna spatial bandwidth, so acting as a low-pass filter. The presented reconstructions have been performed by choosing $p = q = 7$.

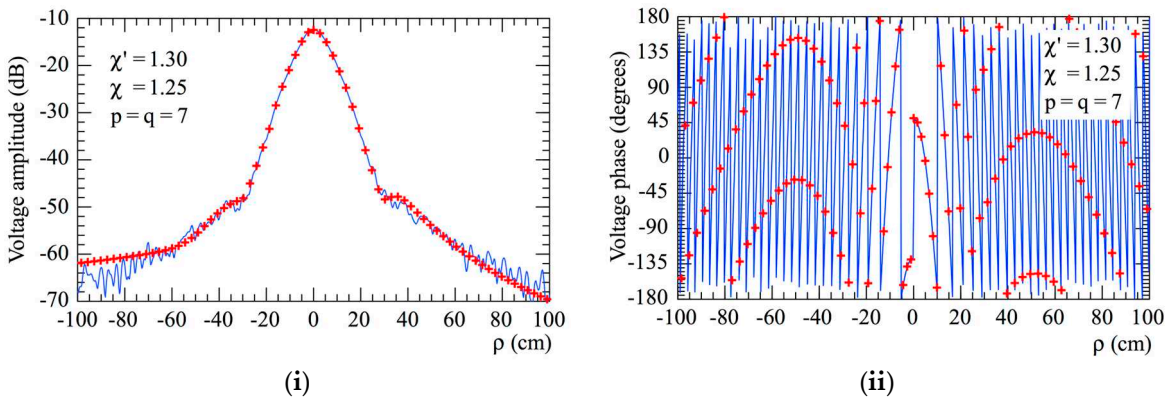

Figure 9. V_φ on the radial line at $\varphi = 0$. —— reference. ++++ got from the planar spiral NF measurements: **(i)** Amplitude; **(ii)** Phase.

Preprints (www.preprints.org) | NOT PEER-REVIEWED | Posted: 3 August 2023 doi:10.20944/preprints202308.0288.v1

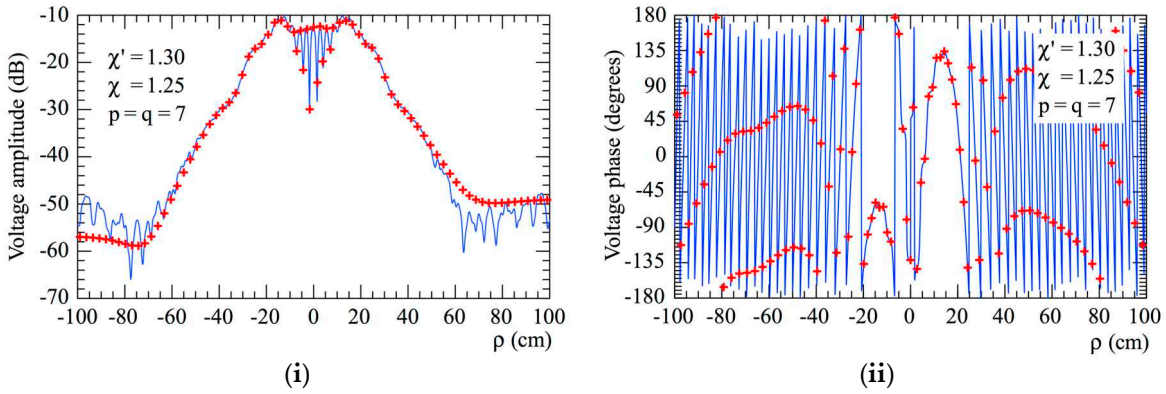

Figure 10. V_ρ on the radial line at $\varphi = \pi/2$. —— reference. ++++ got from the planar spiral NF measurements: (**i**) Amplitude; (**ii**) Phase.

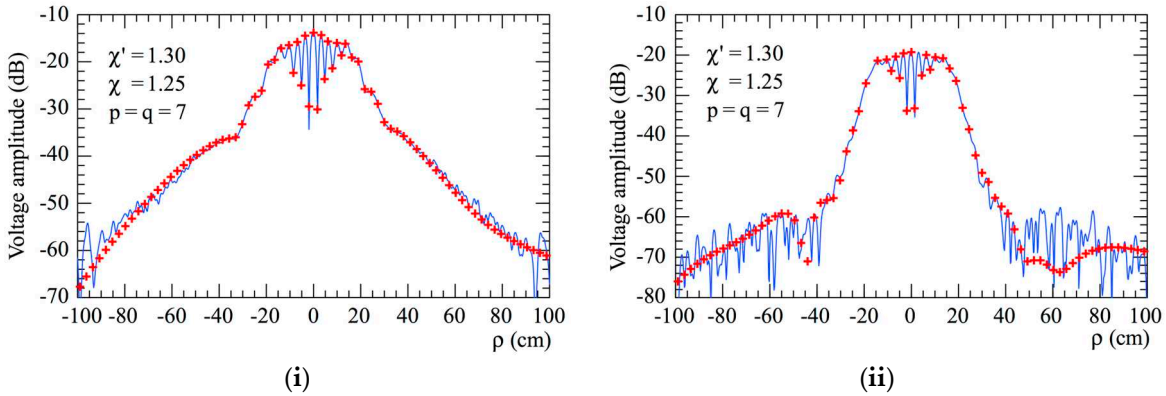

Figure 11. Voltage amplitudes on the radial line at $\varphi = \pi/6$. —— reference. ++++ got from the planar spiral NF samples: (i) Voltage V_φ; (ii) Voltage V_ρ.

Finally, the use of the 2-D OSI expansion followed by the application of equations (17) allows the efficient evaluation of the plane-rectangular data required by the standard Leach & Paris's NF–FF T technique [21] from the voltages V_ρ and V_φ gathered over the spiral. The plane-rectangular sampling lattice adopted for the reconstructions lies on a square having side 140 cm, inscribed in the acquisition circle, and spaced by 0.45λ. The so calculated FF patterns in the principal planes are compared in Figure 12 to those obtained by performing the direct measurements of the NF data at the points of the considered plane-rectangular lattice. It is evident from the reported results as the comparison is fully satisfactory in the E-plane, while that in the H-plane appears less accurate. This occurs since, unlike the open-ended circular waveguide excited by the TE_{11} mode, the far field of an open-ended rectangular waveguide excited by the fundamental mode TE_{10} exhibits only approximately a first-order azimuthal dependence [30]. For the sake of comparison, the FF reconstructions, attained by exploiting the NF spiral samples collected through the hardware co-rotation of the probe, are also presented in Figure 13. In this case, a precise reconstruction of the radiated FF pattern is achieved in both the principal planes.

Preprints (www.preprints.org) | NOT PEER-REVIEWED | Posted: 3 August 2023 doi:10.20944/preprints202308.0288.v1

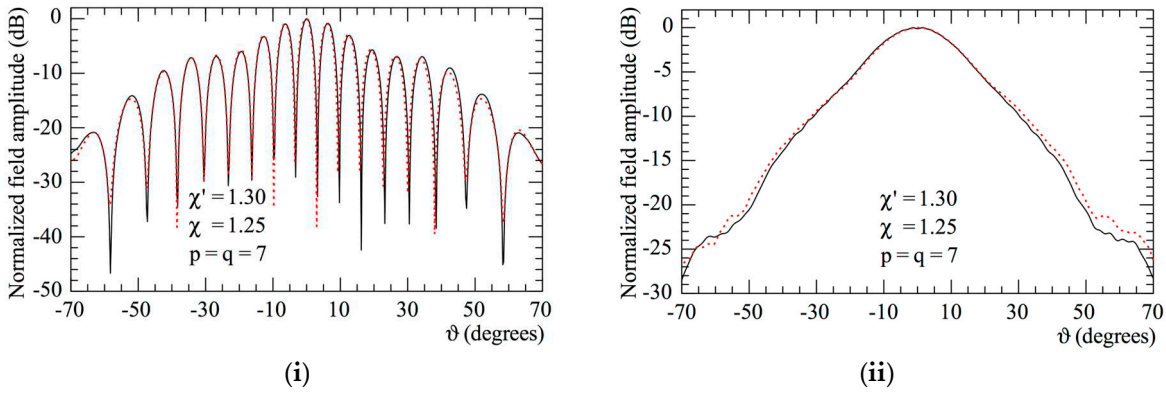

Figure 12. Far-field patterns. ——— reference. - - - - got from the non-redundant samples. Software co-rotation: (**i**) E-Plane; (**ii**) H-plane.

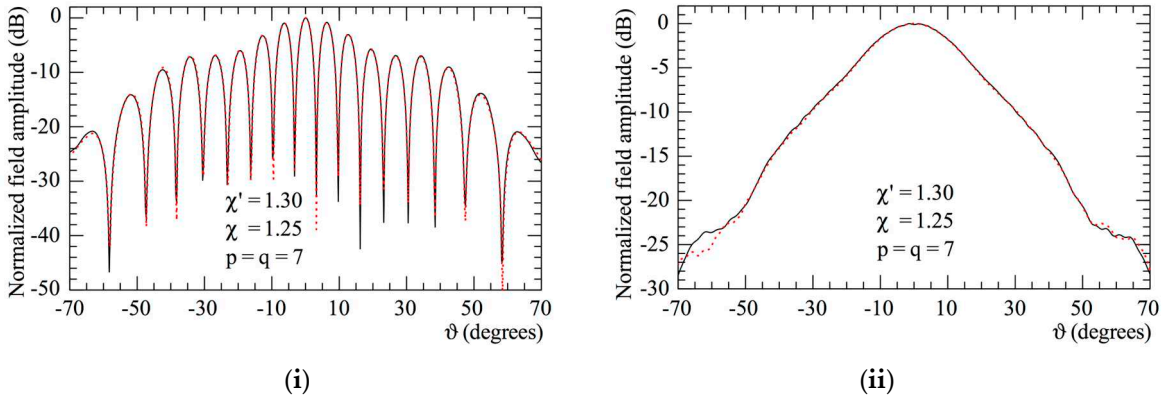

Figure 13. Far-field patterns. ——— reference. Hardware co-rotation - - - - reconstructed from the non-redundant measurements: (**i**) E-Plane; (**ii**) H-plane.

At last, the data reduction obtainable by employing the disk modeling of the AUT is summarized in Table 2. Once again, the amount of NF measurements necessary for the proposed NF–FF T technique is considerably smaller than that necessary to apply the Leach & Paris's transformation [21] and the classical plane-polar NF–FF T technique [31,32]. Moreover, the proposed NF–FF T technique compares favorably with the previous approaches [25,26] for quasi-planar AUTs both from the reduction of needed samples and computational simplicity viewpoints. Note that the number of plane-rectangular samples is the one needed to cover the inscribed $140\,\text{cm} \times 140\,\text{cm}$ sized square, whereas the others numbers are those required by the various techniques to cover the same scanning circle. Moreover, the semi-minor and semi-major axes of the oblate spheroid considered in the comparison are 18.6 cm and 6.0 cm, respectively, whilst the aperture radius of the two-bowls is 18.6 cm and the radii of the upper and lower lateral bends are both 2.4 cm.

Table 2. NF data necessary for the different NF–FF T techniques.

Plane-rectangular NF–FF T [21]	Plane-polar NF–FF T [31,32]	Planar spiral NF–FF T [25,26] Oblate spheroid	Planar spiral NF–FF T [26] Double bowl	Planar spiral NF–FF T Disk
10816	36177	1812	1780	1665

The interested reader can find another set of experimental results validating the efficacy of the proposed technique and relevant to a diverse AUT in [33].

Preprints (www.preprints.org) | NOT PEER-REVIEWED | Posted: 3 August 2023 doi:10.20944/preprints202308.0288.v1

4. Conclusions

In this article, an efficient NF–FF T technique for flat AUTs, which adopts the planar spiral scanning, has been developed and thoroughly assessed both numerically and experimentally. It relies on the application of the non-redundant sampling representations to the probe voltage and has been got by assuming a flat antenna as contained in a disk and exploiting the unified theory of spiral scannings for non-volumetric AUTs. An effective OSI algorithm allows the accurate evaluation of the massive NF data necessary for the Leach & Paris's classical transformation [21] from the non-redundant ones gathered on the spiral. It must be stressed that, in the case of flat antennas, such a NF–FF T technique with planar spiral scan allows a further significant decrease of the acquisition time as compared to the previous ones, wherein the antenna is modeled by a two-bowls or by an oblate spheroid. The numerical NF and FF recoveries have proved the accuracy of the transformation, whereas its practical feasibility has been assessed by the very good agreements obtained in the experimental proofs.

Funding: No external funding has been received for this research.

Conflicts of Interest: The authors declare no conflict of interest.

References

1. Bucci, O.M.; Gennarelli, C.; Savarese, C. Representation of electromagnetic fields over arbitrary surfaces by a finite and nonredundant number of samples. *IEEE Trans. Antennas Propag*. **1998**, *46*, 351-359.
2. Bucci, O.M.; Gennarelli, C. Application of nonredundant sampling representations of electromagnetic fields to NF-FF transformation techniques. *Int. J. Antennas Propag*. **2012**, *2012*, 1–14.
3. Yaghjian, A.D. An overview of near-field antenna measurements. *IEEE Trans. Antennas Propag*. **1986**, *AP-34*, 30–45.
4. Appel-Hansen, J.; Dyson J.D.; Gillespie, E.S.; Hickman, T.G. Antenna measurements. In *The Handbook of Antenna Design*, Rudge, A.W., Milne, K., Olver, A.D., Knight, P., Eds., Peter Peregrinus: London, UK, 1986; pp. 584–694.
5. Gregson, S.F.; McCormick, J.; Parini, C.G. *Principles of Planar Near-Field Antenna Measurements*, IET: London, UK, 2007.
6. Francis, M.H.; Wittmann, R.C. Near-field scanning measurements: theory and practice. In *Modern Antenna Handbook*, Balanis, C.A., Ed.; John Wiley & Sons Inc.: Hoboken NJ, USA, 2008, pp. 929–976.
7. *IEEE Standard 1720-2012 IEEE Recommended Practice for Near-Field Antenna Measurements*; 2012. Francis, M. H. (Ed.) IEEE: New York, NY, USA, 2012.
8. Ferrara, F.; Gennarelli, C.; Guerriero, R. Near-field antenna measurement techniques. In *Handbook of Antenna Technologies*; Chen, Z.N., Liu, D., Nakano, H., Qing, X., Zwick, T., Eds., Springer-Verlag: Singapore, 2016, pp. 2107–2163.
9. Sierra Castañer, M.; Foged, L.J. *Post-processing Techniques in Antenna Measurement*, SciTech Publishing IET: London, UK, 2019.
10. Parini, C.; Gregson, S.; McCormick, J.; Van Resburg, D.J.; Eibert, T. *Theory and Practice of Modern Antenna Range Measurements*, SciTech Publishing IET, London, UK, 2020.
11. Ferrara, F.; Gennarelli, C.; Guerriero, R.; D'Agostino, F. *Non-Redundant Near-Field to Far-Field Transformation Techniques*, SciTech Publishing IET: London, UK, 2022.
12. Ferrara, F.; Gennarelli, C.; Guerriero, R.; Riccio, G.; Savarese, C. An efficient near-field to far-field transformation using the planar wide-mesh scanning. *J. Electromagn. Waves Appl.* **2007**, *21*, 341–357.
13. D'Agostino, F.; De Colibus, I.; Ferrara, F.; Gennarelli, C.; Guerriero, R.; Migliozzi, M. Far-field pattern reconstruction from near-field data collected via a nonconventional plane-rectangular scanning: experimental testing. *Int. J. Antennas Propag*. **2014**, *2014*, 1–9.
14. Bucci, O.M.; Gennarelli, C.; Riccio, G.; Savarese, C. Near-field–far-field transformation from nonredundant plane-polar data: effective modellings of the source. *IEE Proc. Microw. Antennas Propag*. **1998**, *145*, 33–38.
15. Bucci, O.M.; D'Elia, G.; Migliore, M.D. Advanced field interpolation from plane-polar samples: experimental verification. *IEEE Trans. Antennas Propag*. **1998**, *46*, 204–210.
16. D'Agostino, F.; Ferrara, F.; Gennarelli, C.; Guerriero, R.; Migliozzi, M. Far-field pattern reconstruction from a nonredundant plane-polar near-field sampling arrangement. *IEEE Antennas Wirel. Propag. Lett.*, **2016**, *15*, 1345–1348.
17. D'Agostino, F.; Ferrara, F.; Gennarelli, C.; Guerriero, R.; Migliozzi, M. Reconstruction of the antenna far-field pattern through a fast plane-polar scanning. *Appl. Comp. Electromagn. Society J.* **2016**, *31*, 1362-1369.
18. D'Agostino, F.; Ferrara, F.; Gennarelli, C.; Guerriero, R.; Migliozzi, M. Fast and accurate far-field prediction by using a reduced number of bipolar measurements. *IEEE Antennas Wirel. Propag. Lett.* **2017**, *16*, 2939–2942.

Preprints (www.preprints.org) | NOT PEER-REVIEWED | Posted: 3 August 2023 doi:10.20944/preprints202308.0288.v1

19. D'Agostino, F.; Ferrara, F.; Gennarelli, C.; Guerriero, R.; Migliozzi, M. Laboratory tests on a near-field to far-field transformation technique from non-redundant bi-polar data. *IET Microw. Antennas Propag.* **2018**, *12*, 712–717.
20. Paris, D.T.; Leach, W.M., Jr.; Joy, E.B.; Basic theory of probe-compensated near-field measurements. *IEEE Trans. Antennas Propag*. **1978**, *AP-26*, 373–379.
21. Joy, E.B.; Leach, W.M.; Rodrigue, G.P.; Paris, D.T. Applications of probe-compensated near-field measurements. *IEEE Trans. Antennas Propag*. **1978**, *AP-26*, 379–389.
22. Yaccarino, R.G.; Williams, LI.; Rahmat-Samii, Y. Linear spiral sampling for the bipolar planar antenna measurement technique. *IEEE Trans. Antennas Propag*. **1996**, *44*, 1049–1051.
23. Bucci, O.M.; D'Agostino, F .; Gennarelli, C.; Riccio, G.; Savarese, C. Probe compensated far-field reconstruction by near-field planar spiral scanning. *IEE Proc. Microw. Antennas Propag.* **2002**, *149*, 119–123.
24. D'Agostino, F.; Ferrara, F.; Gennarelli, C.; Guerriero, R.; Migliozzi, M. A planar NF–FF tranformation for quasi-spherical antennas using the innovative spiral scanning. *Appl. Comp. Electromagn. Society J.* **2018**, *33*, 115–118.
25. D'Agostino, F.; Ferrara, F.; Gennarelli, C.; Guerriero, R.; Migliozzi, M. An effective NF-FF transformation technique with planar spiral scanning tailored for quasi-planar antennas. *IEEE Trans. Antennas Propag.* **2008**, *56*, 2981–2987.
26. D'Agostino, F.; Ferrara, F.; Gennarelli, C.; Guerriero, R.; McBride, S.; Migliozzi, M. Fast and accurate antenna pattern evaluation from near-field data acquired via planar spiral scanning. *IEEE Trans. Antennas Propag.* **2016**, *64*, 3450–3458.
27. D'Agostino, F.; Gennarelli, C.; Riccio, G.; Savarese, C. Theoretical foundations of near-field–far-field transformations with spiral scannings. *Prog. Electromagn. Res.* **2006**, *61*, 193–214.
28. D'Agostino, F.; Ferrara, F.; Gennarelli, C.; Guerriero, R.; Migliozzi, M. The unified theory of near–field–far–field transformations with spiral scannings for nonspherical antennas. *Prog. Electromagn. Res. B*. **2009**, *14*, 449–477.
29. Cicchetti, R.; D'Agostino, F.; Ferrara, F.; Gennarelli, C.; Guerriero, R.; Migliozzi, M. Near-field to far-field transformation techniques with spiral scannings: a comprehensive review. *Int. J. Antennas Propag*. **2014**, *2014*, 1–13.
30. Yaghjian, A.D. Approximate formulas for the far field and gain of open-ended rectangular waveguide. *IEEE Trans. Antennas Prop*. **1984**, *AP-32*, 378–384.
31. Rahmat-Samii, Y.; Galindo-Israel, V.; Mittra, R. A plane-polar approach for far-field construction from near-field measurements. *IEEE Trans. Antennas Propag*. **1980**, *AP-28*, 216-230.
32. Gatti, M.S.; Rahmat-Samii, Y. FFT applications to plane-polar near-field antenna measurements. *IEEE Trans. Antennas Propag*. **1988**, *36*, 781-791.
33. Bevilacqua, F.; D'Agostino, F.; Ferrara, F.; Gennarelli, C.; Guerriero, R.; Migliozzi, M. ; Riccio, G. Experimental testing of an effective near to far-field transformation for flat antennas using non-redundant spiral data. In Proc. of European Conference on Antennas & Propagation, EUCAP 2022, Madrid, Spain, 2022; pp. 1-5.

Disclaimer/Publisher's Note: The statements, opinions and data contained in all publications are solely those of the individual author(s) and contributor(s) and not of MDPI and/or the editor(s). MDPI and/or the editor(s) disclaim responsibility for any injury to people or property resulting from any ideas, methods, instructions or products referred to in the content.